Modeling of processes during pulsed-laser texturing of material surfaces

Vatsya, S.R.; Nikumb, S.K.

Publisher's version / Version de l'éditeur:
https://doi.org/10.1103/PhysRevB.68.035410
Physical Review. B, Condensed Matter and Materials Physics, 68, 2003-07-15

Modeling of processes during pulsed-laser texturing of material surfaces

S. R. Vatsya and S.K. Nikumb

Integrated Manufacturing Technologies Institute
National Research Council of Canada
800 Collip Circle, London, ON, Canada, N6G 4X8

Abstract

Pulsed-laser texturing of material surfaces proceeds with shallow melt resulting from the absorption of laser energy. Flow processes in the fluid determine the morphological structure of the re-solidified surface. Approximations made in the literature are improved upon here to describe the fluid flow in the melt. In particular, the pressure in the melt is included in the Navier-Stokes equation and the surface boundary condition, which is shown to have significant impact on the flow processes and thus, on the final finish of the surface. The calculations for Si surface modifications are found to be in close agreement with the experimental observations, considerably improving upon the earlier descriptions.

PACS number(s): 68.03.Cd, 66.20.+d, 65.20.+w, 42.62.-b

I. INTRODUCTION

Since its demonstration[1] for NiP_x, laser zone texturing has become a frequently used technique for micron-scale modifications to obtain the desired surface properties for its advantage in producing cleaner surfaces without damage to the substrate. Irradiation of metals, semi-metals and semiconductors with lasers of pulse-widths in the nanosecond range creates a molten region close to the surface. With sufficiently high intensities, the material is removed by evaporation[2-5]. For lower intensities, the energy absorbed by the molten material generates inhomogeneous temperature distribution creating gradient in the surface tension, which can drive the fluid from the center of the melt pool to its outer periphery. The final shape of the re-solidified material is determined by the detailed hydrodynamic properties of the melt. Experimentally, bowl-like craters on the surface of depth of one to few hundred nanometers and diameter from one to several micrometers, with a rim at the boundary raised a few nanometers above the surface are observed[6,7]. Reliance on the fluid flow properties makes it possible to make modifications to the surface morphology at a finer scale than the techniques based on material removal[8]. This procedure also avoids contamination, which may result from the processes dependent on etching and lithography as well as substrate damage, which may result by techniques based on ablation. In case of irradiation with pulse-widths in the sub-picoseconds range, material removal occurs without passing through the melting phase.[9-10] Thus, low intensity lasers with long pulse-widths are better suited for texturing.

Motivated by its dependence on the hydrodynamic behavior of the melt, standard equations of fluid flow were used, in Ref. [7], to describe the changes in the surface morphology of Si. Analysis was simplified by neglecting the terms, which were considered to be small for large values of the viscosity. Also, some approximations were made to simplify the calculations. The calculated shape of the dimple with peak laser energy of $0.82\ J/cm^2$ was found to be in close agreement with the experimentally observed surface profile with peak laser energy of $1.1\ J/cm^2$. Thus, the model under-estimates the energy required by about 25%. It is shown in the present note that there is considerable pressure build up in the melt, which was neglected in the earlier model[7]. It is shown here that the pressure has a significant impact on the fluid velocities, which determine the structure of the re-solidified surface. Inclusion of the pressure in the model together with improved solutions is shown to improve the agreement between the theoretical and the experimental values considerably for the test case of Si. To be precise, the theoretical values with peak laser energy of $1.15\ J/cm^2$ were found to be in close agreement with the experimental values with $1.1\ J/cm^2$, thus bringing the agreement to within 5%.

The method developed and the results obtained here also apply to the cases of material removal by laser irradiation. Advances in micro-machining technology have made it possible to remove material to fabricate sub-micron scale features using lasers. Models have been developed to understand the relation between the process parameters and the geometrical profile of the craters[5]. These models ignore the phenomena in the thin melt that exists between the ablated surface and the solid substrate for their complexity, and approximate the laser-material interaction by coupling the evaporation phase and the heat transfer to the material below the melt. An understanding of the fluid flow in the melt will improve these models considerably by enabling the inclusion of the melt behavior to describe the surface profile more accurately.

The model equations describing the phenomena in the melt pool are developed in Sec. II. Sufficiently accurate solutions to these equations are obtained in Sec. III, which are used in Sec. IV to calculate the change in the surface morphology for the test case of Si.

II. FLUID FLOW MODEL

Surface temperatures of metals, semimetals and semiconductors irradiated with lasers reach the melting point soon after the exposure to radiation begins[2-5,11]. With intensities insufficient to evaporate the material and still maintain the heat diffusion into the material, thermal equilibrium is reached between the environment, melt and the solid. The energy is then used in maintaining the equilibrium with associated inhomogeniety in the temperature distribution in the melt. Thus, the behavior of the fluid in case of laser texturing can be adequately described by the steady state fluid flow equations, which will be assumed in the following. Additional simplifying assumptions will be made as long as they are realistic.

For an incompressible fluid, the steady state continuity equation for the fluid velocity υ reduces to

$$\nabla \cdot \upsilon = 0 \tag{1}$$

and the Navier-Stokes equation[12] can be approximated with

$$\nabla^2 \upsilon - \frac{1}{\eta} \nabla P = 0 \tag{2}$$

where η is the dynamic viscosity and P is the pressure in the melt. In addition to assuming the steady state, Eq. (1) has been used and the nonlinear term, which is directly proportional to $(\upsilon \cdot \nabla \upsilon)$, has been neglected in deducing Eq. (2). The external force is also excluded from Eq. (2), which in the present case is only gravitational having little effect, particularly if the textured surface is horizontal. Furthermore, the pressure will be obtained below as a solution of the Laplace equation, and thus the force term can be absorbed in the pressure.

An independent equation for the pressure can be obtained by taking the divergence of Eq. (2) and using Eq. (1), which yields,

$$\nabla^2 P = 0 \tag{3}$$

Since the surface is horizontal and the laser beam is radially symmetric, the velocities and the pressure will be assumed radially symmetric, and the cylindrical coordinate system will be used for its suitability for the present system. Let h denote the melt-depth. The velocity at the bottom of the melt is equal to zero, i.e., $\upsilon_r(-h,r) = \upsilon_z(-h,r) = 0$, where $\upsilon_r(z,r)$ and $\upsilon_z(z,r)$ are the radial and vertical components of the velocity. The surface boundary condition is given by[13],

$$\frac{\partial \upsilon_z}{\partial r} + \frac{\partial \upsilon_r}{dz} - \frac{1}{\eta} P = \frac{1}{\eta} \frac{\partial \alpha}{\partial r}, \quad z = 0, \tag{4}$$

where α is the surface tension and the value of the pressure P is taken relative to its value above the surface.

The present model differs from an earlier one[7] in that the pressure is included in the Navier-Stokes equation and the surface boundary condition. Since the velocity components are zero at the interface of the fluid and the solid, i.e., at the bottom of the melt, there is nonzero velocity gradient in the fluid. Also, the fluid is assumed to be incompressible. Close to $r = 0$, the gradient in the vertical direction causing the slip can be absorbed in the radial component of the velocity. However, the radial component of the velocity also possesses nonzero gradient, and thus, there must be significant pressure buildup for larger values of the radial coordinate. These phenomenological observations and the justification for neglecting the nonlinear term in deducing Eq. (2) will become more transparent from the analysis of Sec. III.

III. FLUID PRESSURE AND THE VELOCITIES

In this section, approximate solutions to the model equations developed in Sec. II are obtained. The aim here is to determine the leading term in the expansion of $v_z(z,r)$ in powers of $[(z+h)/r_{max}]$, where r_{max} is the maximum radius of the melt. To determine the leading term for $v_z(z,r)$ it was found necessary to obtain some other quantities more accurately, as will be seen below. The melt depth h depends on the radial location. However, its absolute value is quite small compared to the radius of the molten region, which also indicates that its variation with respect to the radial coordinate is small compared to its absolute value. Therefore, the terms of the order of (h/r_{max}) and the variation of $h(r)$ with respect to r in comparison with h are neglected without further mention. Since $|(z+h)| \leq h$, accuracy of the velocity is consistent with this approximation. As others, these approximations result in considerable simplifications without significant impact on the accuracy of the solutions. Time integral of $v_z(0,r)$ over the pulse-width yields the value of the modification Δz to the morphological structure of the material surface in terms of the melt depth h, which can be calculated by the methods available elsewhere[2-5].

Eq. (3) can be solved by the method of the separation of variables[14], i.e., by expressing the solution $P(z,r)$ as $P(z,r) = u(z)w(r)$. This decomposes Eq. (3) into

$$\frac{d^2u(z)}{dz^2} = \lambda^2 u(z) \tag{5}$$

and the zero order Bessel equation:

$$\frac{d^2w(r)}{dr^2} + \frac{1}{r}\frac{dw(r)}{dr} = -\lambda^2 w(r) \tag{6}$$

A general form of the solution of Eq. (5) is given by,

$$u(z) = \left(a \cosh[\lambda(z+h)] + b \sinh[\lambda(z+h)]\right)$$

where a and b are constants. Since $P(z,r)$ is finite, it follows from Eq. (6) that[14] $w(r) = J_0(\lambda r)$, within a multiplicative constant, which can be absorbed in a and b in the representation of $P(z,r)$. Here, $J_0(\lambda r)$ is the zero order Bessel function[14]. Since r_{max} must be at or outside the boundary of the melt, it can be assumed that $P(z, r_{max}) = 0$, which determines the parameter λ from $J_0(r_{max}\lambda) = 0$. Although the precise value of r_{max} is not known, the fact that it is finite is sufficient to conclude that the values $\{\lambda_n\}$ of λ form a positive, discrete, infinite set. The complete solution for $P(z,r)$ is given by

$$P(z,r) = \eta \sum_{n=0}^{\infty} \left(a_n \cosh[\lambda_n (z+h)] + b_n \sinh[\lambda_n (z+h)] \right) J_0(\lambda_n r) \tag{7}$$

where a_n and b_n are as yet undetermined constants. The viscosity η is explicitly included in the solution for convenience. The form of the solution for the pressure given by Eq. (7), together with Eq. (2), will be used as the guiding form in obtaining the solutions for the velocities below.

Since $\{J_0(\lambda_n r)\}$ forms a complete set, $v_z(z,r)$ can be expressed as

$$v_z(z,r) = \sum_{n=0}^{\infty} \phi_n(z)\, J_0(\lambda_n r) \tag{8}$$

Using the relation $[\partial J_o(\lambda r)/\partial r = -\lambda J_1(\lambda r)]$ together with Eq. (6) satisfied with $\lambda = \lambda_n$ for each n, yields an alternative form of $v_z(z,r)$ given by,

$$v_z(z,r) = \sum_{n=0}^{\infty} \phi_n(z)\, \frac{1}{\lambda_n r} \frac{\partial}{\partial r} (r J_1(\lambda_n r)) \tag{9}$$

Substitution for $v_z(z,r)$ from Eq. (9) in the continuity equation, Eq. (1), results in

$$v_r(z,r) = -\sum_{n=0}^{\infty} \frac{1}{\lambda_n} \frac{\partial \phi_n(z)}{\partial z} J_1(\lambda_n r) \tag{10}$$

Since the components of the velocity vanish at $z = -h$, it follows that $\phi_n(-h) = 0$ and $\partial \phi_n(z)/\partial z = 0$ at $z = -h$. Let

$$\frac{\partial \phi_n(z)}{\partial z} = \lambda_n \left\{ c_n \sinh[\lambda_n (z+h)] + d_n \left(\cosh[\lambda_n (z+h)] - 1 \right) \right\},$$

and thus,

$$\phi_n(z) = \left\{ c_n \left(\cosh[\lambda_n (z+h)] - 1 \right) + d_n \left(\sinh[\lambda_n (z+h)] - \lambda_n (z+h) \right) \right\} \tag{11}$$

The continuity equation, Eq. (1), is exactly solved by v_z and v_r as defined by Eqs. (8) and (10), respectively, with ϕ_n defined by Eq. (11).

Substitution for v_z in Eq. (2) yields,

$$\sum_{n=0}^{\infty}\left\{\lambda_n c_n - \lambda_n^2(z+h)d_n - a_n \sinh[\lambda_n(z+h)] - b_n \cosh[\lambda_n(z+h)]\right\} J_0(\lambda_n r) \;=\; 0 \qquad (12)$$

Since $\{J_0(\lambda_n r)\}$ forms an orthogonal set, coefficient of $J_0(\lambda_n r)$ must be zero for each n. With $c_n = b_n/\lambda_n$ and $d_n = a_n/\lambda_n$, Eq. (12) is solved approximately, with the error being of the order of $[(z+h)/r_{\max}]^2$. By substitution for v_r in the corresponding Navier-Stokes equation, it can be seen that the equation is solved with the same values of these constants, but with the error being of the order of $[(z+h)/r_{\max}]$. However, this is sufficiently accurate for the present purpose.

Substitution for the appropriate quantities in Eq. (4) now reduces it to

$$\sum_{n=0}^{\infty}[a_n J_0(\lambda_n r) + b_n J_1(\lambda_n r)] + \frac{1}{\eta}\frac{\partial \alpha}{\partial r} = 0 \qquad (13)$$

where the terms of the order of $(h/r_{\max})$ and higher are dropped in consistency with the accuracy of the solutions. Approximate solution to Eq. (13) can be obtained by minimizing the norm of the left side together with truncating the sum at a finite number N, instead of infinite. To be precise, the scalar product (u,w) given by

$$(u,w) \;=\; \int_0^{r_{\max}} dr\, r\, u(r) w(r)$$

defines the Hilbert space of functions of r on the interval $[0, r_{\max}]$, consistent with the cylindrical coordinate system. Minimizing the norm reduces Eq. (13) to a set of $2(N+1)$ algebraic equations as follows. Let $\psi_n(r) = J_0(\lambda_n r)$, $\xi_n = a_n$, $\psi_{(N+n+1)}(r) = J_1(\lambda_n r)$ $\xi_{(N+n+1)} = b_n$, for $n = 0$ to N. Define a matrix A with elements A_{nm} given by $A_{nm} = (\psi_n, \psi_m)$, $n, m = 0,1,\ldots,(2N+1)$, and vectors ξ and γ with elements ξ_n and $\gamma_n = (\psi_n, \beta)$, where $\beta(r) = -(\partial\alpha/\partial r)/\eta$. The vector ξ is determined by solving the matrix equation

$$A\xi \;=\; \gamma \qquad (14)$$

Retaining the leading terms, approximate values of the components of the velocity are given by

$$v_z(z,r) \;=\; \frac{1}{2}(z+h)^2 \sum_{n=0}^{N} b_n \lambda_n J_0(\lambda_n r) \qquad (15)$$

$$v_r(z,r) = -(z+h)\sum_{n=0}^{N} b_n J_1(\lambda_n r) \tag{16}$$

and the pressure in the melt is given by

$$P(z,r) = \eta\sum_{n=0}^{N} a_n J_0(\lambda_n r) \tag{17}$$

It is clear from Eqs. (13) and (14) that a_n and b_n are of the order of $(1/\eta)$. Eqs. (15) and (16) now imply that the velocity is of the order of $(1/\eta)$. Consequently, the terms quadratic in the velocity are negligible compared to the velocity for large values of the viscosity, justifying the corresponding approximation in deducing the approximate form of the Navier-Stokes equation, Eq. (2). Further, from Eq. (17) it follows that substantial amount of pressure develops in the melt having a significant impact on the behavior of the fluid. Also, it can be seen from Eq. (13) that the inclusion of the pressure term tends to reduce the absolute values of the velocity components, and thus a given intensity laser would modify the surface morphology to a lesser extent in comparison with the value obtained by neglecting the pressure.

IV. RESULTS AND DISCUSSION

The change in the morphology of the surface is given by the time integral of $v_z(0,r)$. Thus, Eq. (15) yields,

$$\Delta z(r) = \frac{1}{2}\sum_{n=0}^{N}\int_{T>T_{melt}} h^2(r,t) b_n(t)\lambda_n J_0(\lambda_n r)dt \tag{18}$$

where T_{melt} is the melting point. Following the argument of Ref. [7], the derivative of the surface tension will be expressed as,

$$\frac{\partial\alpha}{\partial r} = \frac{\partial\alpha}{\partial T}\frac{\partial T}{\partial r},$$

where $(\partial\alpha/\partial T)$ is constant. It follows from Eq. (13) that the behavior of $\xi_n(t)$, and thus, of $a_n(t)$ and $b_n(t)$, is the same as that of $T(t)$, which is more strongly peaked than $h(t)$. The modification $\Delta z(r)$ can be further approximated to a good degree of accuracy by[7]

$$\Delta z(r) = \frac{1}{2}\sum_{n=0}^{N}\langle h^2\rangle(r)\langle b_n\rangle\lambda_n J_0(\lambda_n r) \tag{19}$$

where $\langle\ \rangle$ denotes the value integrated with respect to time for the duration of the pulse-width. Thus, it is sufficient to calculate $\langle\xi\rangle$ instead of the vector ξ itself. The vector $\langle\xi\rangle$ can be obtained by replacing ξ and γ in Eq. (14) by $\langle\xi\rangle$ and $\langle\gamma\rangle$, where $\langle\gamma_n\rangle = (\psi_n, \langle\beta\rangle)$. The value $\langle\beta\rangle(r)$ is obtained from the time-integrated value I of the temperature given by

$$I = \int_{T>T_{melt}} [T(t) - T_{melt}]\, dt$$

yielding

$$\langle \beta \rangle (r) = -\frac{1}{\eta} \frac{\partial \alpha}{\partial T} \frac{\partial I}{\partial r}.$$

Integrated melt depth, also needed to determine the modification to the surface morphology is determined by

$$\langle h^2 \rangle I = \int_{T>T_m} dt\ (T - T_m)\ h^2.$$

Eq. (14) modified as above also determines the time-integrated pressure, which is obtained by replacing a_n by $\langle a_n \rangle$ in Eq. (17). The values of I and $\langle h^2 \rangle$ can be computed as functions of the intensity $F(r)$. This determines them as functions of the radial coordinate r from the knowledge of the functional dependence of the intensity on r[7].

For comparison, the experimental values, and the other data was taken from Ref. [7] to calculate Δz from Eq. (19), reported in Figures (1) and (2). The variable $r_{\max}$ was set equal to $1.5\ \mu m$ and $N = 6$. However, the value of $r_{\max}$ had no noticeable effect on the final values as long as it was larger than the melt radius, and the truncation at $N = 4$ was found to be quite satisfactory.

Figure 1 compares the values of Δz as determined by Eq. (11) of Ref. [7] for the peak intensity $F(0) = 0.82\ J/cm^2$, and as determined by the present Eq. (19) for $F(0) = 1.15\ J/cm^2$, with the experimentally observed values, reported in Ref. [7] for $F(0) = 1.1\ J/cm^2$. All the three values are quite close to each other. The present values, (II), approximate the rim noticeably better than Ref. [7]. Thus, the present result reduces the discrepancy between the experimental and the theoretical values, in terms of the peak intensity, to within 5%, from about 25% of Ref. [7] and improves the resolution of the rim.

Figure 2 compares the values calculated from Eq. (19), with $F(0) = 1.1\ J/cm^2$ and $F(0) = 1.2\ J/cm^2$, with the experimentally measured values for $F(0) = 1.1\ J/cm^2$. The calculated values with $F(0) = 1.1\ J/cm^2$ underestimate the maximum melt-depth as well as the height of the rim. The values with $F(0) = 1.2\ J/cm^2$ overestimate the melt-depth over a wider range, as well as the height of the rim. The experimental values are bounded by these two sets of values, almost over the entire range. Above conclusions are based on the assumption that the experimental values are completely free of errors and uncertainties, which is unlikely. In any case, the present analysis and calculations demonstrate that the inclusion of the pressure improves the model considerably.

Figure 3 shows the time-integrated pressure in the melt in units of its viscosity, which is constant with respect to the z coordinate within the present approximation. As expected from the phenomenological considerations, the pressure is almost equal to zero close to the origin,

which is equal to the atmospheric plus the vapor pressure on the present scale, increasing in magnitude closer to the rim and falling back to zero as the melt depth diminishes.

V. CONCLUDING REMARKS

Need for an adequate understanding of the processes in the molten material arises in pulsed-laser texturing as well as in ablation of materials with lasers of long pulse-widths. Micro-modification to the surface morphology is described almost entirely by the behavior of the melt. In case of ablation, the thin melt that exists between the ablated surface and the solid substrate affects the surface profile as indicated by observations of the craters formed by laser irradiation[5]. A model is developed here, which adequately describes the phenomena in the melt for small values of the melt depth in comparison with the melt radius. Significant pressure build up takes place in the fluid as a consequence of the velocity gradient, which in turn impacts upon the values of the velocity components, thereby affecting the modifications to the surface morphology. For the test case of Si, inclusion of the pressure in the Navier-Stokes equation and the surface boundary condition is found to improve the agreement between the calculated and observed values of the modifications to the surface morphological structure considerably. While the shallow melt case considered here covers large number of cases encountered in laser texturing and machining, further improvements will be required for deeper melt cases. However, the present solution scheme provides a foundation to treat such cases also.

Acknowledgements

Thanks are due to Mr. M. Islam, Director, Production Technology Research, IMTI, for his continued support in this work. Assistance of Ingrid Koslow with the preparation of the manuscript is also gratefully acknowledged.

References

[1] R. Ranjan, D.N. Lambeth, M. Tromel, P. Goglia, and Y. Li, J. Appl. Phys. **69** 5745 (1991).

[2] R.F. Wood, C.W. White and R.T. Young, Laser processing of semiconductors: An overview, in Semiconductors and semimetals, Vol. **23** (Academic Press, New York, 1984) pp.1-41.

[3] R.F. Wood and G.E. Jellison, Jr., Melting model of pulsed laser processing, in Semiconductors and semimetals, Vol. **23** (Academic Press, New York, 1984) pp.166-250.

[4] R.F. Wood and G.E. Giles, Macroscopic theory of pulsed-laser annealing. I. Thermal transport and melting. Phys. Rev. B **23**, 1981; pp. 2923-2942.

[5] S.R. Vatsya, E.V. Bordatchev and S.K. Nikumb, Geometrical modeling of surface profile formation during laser ablation of materials , J. App. Phys. Submitted for publication.

[6] S.C. Chen, D.G. Cahill, and C.P. Grigoropoulos, J. Heat Transfer **122**,107 (2000).

[7] T. Schwarz-Selinger, D.G. Cahill, S.C. Chen, S.J. Moon and C.P. Grigoropoulos, Phys. Rev. B **64,** 15 5323 (2001).

[8] H.K. Park, P.I.M. Kerstens, P. Baumgart and A.C. Tam, IEE Trans. Magn. **34**, 1807(1998).

[9] B.N. Chichkov, C. Momma, S. Nolte, F. von Alvensleben and A. Tunnermann, Femtosecond, picosecond and nanosecond laser ablation of solids. Appl. Phys. A. 63: 1996; pp. 109-115.

[10] S. Nolte, C. Momma, H. Jacobs, A. Tunnermann, A., B.N. Chichkov, B. Wellegehausen and H. Welling, Ablation of metals by ultrashort laser pulses. J. Opt. Soc. Am. B. 14: 1997; pp. 2716-2722.

[11] S.R. Vatsya and Kuljit S. Virk, Solution of two-temperature thermal diffusion model of laser-metal interactions, Submitted for publication.

[12] See, e.g., K. Huang, *Statistical Mechanics*, (John Wiley & sons, Inc., New York, 1963) p. 112.

[13] See, e.g., L.D. Landau and E.M. Lifshitz, *Fluid Mechanics,* Second edition, (Pergamon Press, New York, 1987) pp.238-241.

[14] R. Courant and D. Hilbert, *Methods of Mathematical Physics*, Vol. I, Third Printing, (Interscience Publishers, Inc., New York, 1961) pp. 302-306.

Figure captions

Figure 1. Comparison of the morphology of a laser dimple created on HF treated Si, as calculated from Eq. (11) of Ref. [7] for $F(0) = 0.82\ J/cm^2$ (I); as measured by AFM for $F(0) = 1.1\ J/cm^2$ (from FIG. 6 of Ref. [7]) (E); and as predicted by Eq. (19) for $F(0) = 1.15\ J/cm^2$ (II).

Figure 2. Comparison of the morphology of a laser dimple created on HF treated Si, as calculated from Eq. (19) for $F(0) = 1.2\ J/cm^2$ (1.2 (II)); as measured by AFM for $F(0) = 1.1\ J/cm^2$ (from FIG. 6 of Ref. [7]) (1.1 (E)); and as predicted by Eq. (19) for $F(0) = 1.1\ J/cm^2$ (1.1 (II)).

Figure 3. Pressure profile (Normalized Pressure = Time integrated pressure/Viscosity) in the laser created melt on the surface of HF treated Si for $F(0) = 1.15\ J/cm^2$.

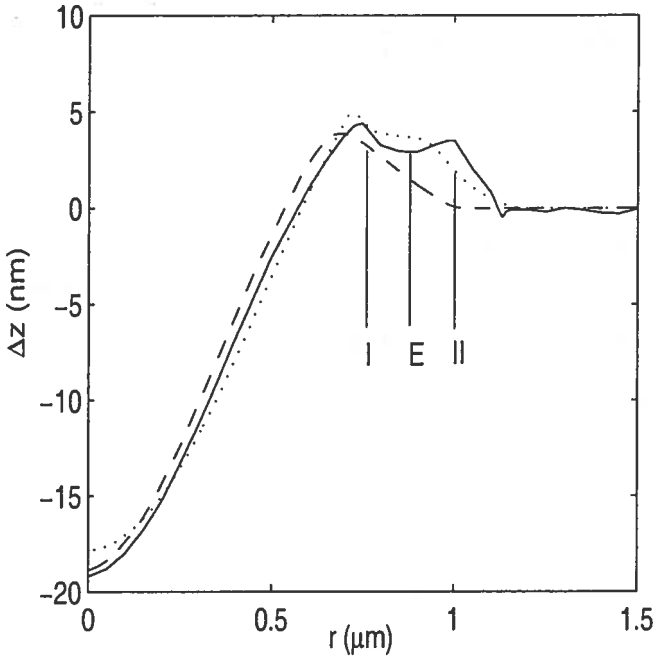

Figure 1.

S. R. Vatsya and S.K. Nikumb

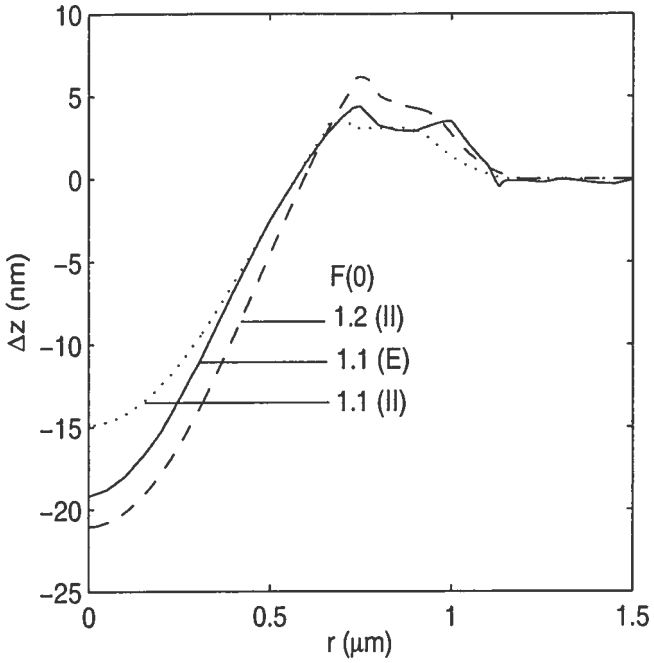

Figure 2.

S. R. Vatsya and S.K. Nikumb

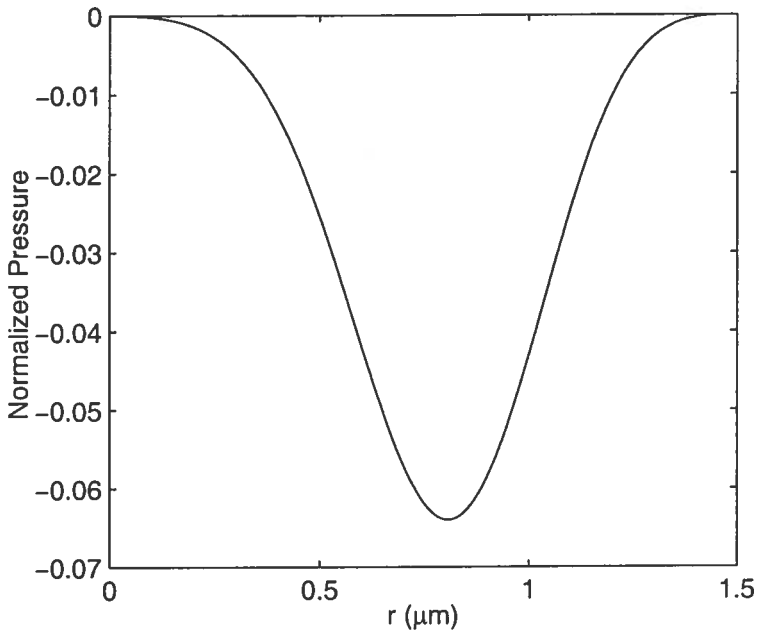

Figure 3.

S. R. Vatsya and S.K. Nikumb